Hierarchy of transcriptomic specialization across human cortex captured by myelin map topography

Joshua B. Burt[1], Murat Demirtaş[2], William J. Eckner[1], Natasha M. Navejar[3], Jie Lisa Ji[4], William J. Martin[5], Alberto Bernacchia[6], Alan Anticevic[2] & John D. Murray[1,2]

[1]*Department of Physics, Yale University, New Haven, CT*
[2]*Department of Psychiatry, Yale University School of Medicine, New Haven, CT*
[3]*Tulane University, New Orleans, LA*
[4]*Interdepartmental Neuroscience Program, Yale University, New Haven, CT*
[5]*BlackThorn Therapeutics*
[6]*University of Cambridge, Cambridge, United Kingdom*

Hierarchy provides a unifying principle for the macroscale organization of anatomical[1–4] and functional[5–8] properties across primate cortex, yet the microscale bases of hierarchical specialization across human cortex are poorly understood. Anatomical hierarchy is conventionally informed by invasively measured laminar patterns of long-range cortico-cortical projections[1–4], creating the need for a principled proxy measure of hierarchy in humans. Moreover, cortex exhibits a transcriptional architecture characterized by distinct profiles of gene expression across areas[9–12], yet organizing principles for areal transcriptomic specialization remain unclear. We hypothesized that functional specialization of human cortical microcircuitry across areas involves hierarchical gradients of gene expression. Here we show that a noninvasive neuroimaging measure, the MRI-derived myelin map[13], indexes the anatomical hierarchy and closely resembles the dominant areal pattern of transcriptomic variation across the human cortex. We found strong hierarchical gradients in expression of genes related to cortical microcircuit function, which we validated with microanatomical data from monkey cortex, and in expression of genes related to neuropsychiatric disorders. These findings establish hierarchy as a general organizing principle, defining an axis shared by the transcriptomic and anatomical architectures of human cortex, and suggest that hierarchical gradients of microscale properties shape the macroscale specialization of cortical function.

Anatomical hierarchy is defined as a globally consistent ordering of cortical areas constrained by characteristic laminar patterns of interareal projections, which have been extensively measured in nonhuman primates[1–3]. The invasive anatomical tract-tracing techniques necessary to conventionally index hierarchy have precluded analogous investigations of cortical organization in humans. We therefore first sought to establish a noninvasive neuroimaging measure that can serve as a proxy for anatomical hierarchy in human and nonhuman primate cortex. One candidate we identified was the cortical myelin map, which can be defined from structural MRI as the contrast ratio of T1- to T2-weighted (T1w/T2w) maps[13]. The myelin map provides a noninvasive *in vivo* measure of gray-matter intracortical myelin content and reflects borders between cytoarchitecturally delineated cortical areas[13]. Myelin map values are high in primary sensory cortex (visual, somatosensory, auditory) and low in association cortex, homologously in human and macaque (Fig. 1a–c, Extended Data Fig. 1). Motivated by these empirical observations, we hypothesized that the myelin map provides a noninvasive proxy for cortical areas' positions along the hierarchy through an inverse relationship.

We can quantitatively validate this proxy measure in macaque cortex through anatomical tract-tracing data of interareal projections with laminar specificity[3]. Laminar connectivity data are used to specify a hierarchical ordering of cortical areas such that lower areas send feedforward projections to higher areas, and higher areas send feedback pro-

jections to lower areas[1–3,14] (Extended Data Fig. 2). Feedforward and feedback projections primarily originate from the supragranular and infragranular layers, respectively. At the level of individual projections, we found that the difference in myelin map values between connected areas is correlated with the laminar feedforward/feedback structure of the connection (Fig. 1d). Globally, we found a strong negative correlation between hierarchy and myelin map values ($r_s = -0.76$, $P < 10^{-5}$; Spearman rank correlation) (Fig. 1e,f). The myelin map was more predictive of hierarchy than were two other candidate neuroimaging measures[15], cortical thickness and distance from primary visual cortex (Extended Data Fig. 3). The strong inverse relationship supports the cortical myelin map as a noninvasive proxy measure for hierarchy which can be applied to human cortex where lack of tract-tracing data prevents direct characterization of hierarchy.

The organizing principles for the large-scale structure of microcircuit specialization across human cortical hierarchy remain unclear. The study of the molecular composition of cortical microcircuitry has been revolutionized by large-scale transcriptomics, which can map expression levels of genes involved in neurobiological processes[9–11]. Datasets such as the Allen Human Brain Atlas (AHBA) have revealed a transcriptomic architecture with distinct gene expression profiles across areas of the human brain[9,10,12]. To test for hierarchical microcircuit specialization across human cortex, we examined areal patterns of cortical gene expression from the AHBA in relation to the myelin map. Due to

the strong inverse relationship observed between the myelin map and hierarchy, if the spatial pattern of gene expression is negatively correlated with the myelin map, then expression level increases along anatomical hierarchy; conversely, a positive correlation indicates decreasing expression along hierarchy. To support the validity of interpretations, we compared the myelin map correlation (MMC) of microcircuitry-related genes in human cortex to more direct anatomical measures in macaque cortex, with focus on cytoarchitecture, inhibitory interneuron densities, and synaptic processes (Fig. 2).

An established feature of microcircuit specialization that varies along cortical hierarchy is the degree of laminar differentiation in cytoarchitecture[4]: primary sensory cortex is highly laminated with a well-defined granular layer, whereas association cortex is characterized by decreasing laminar differentiation and a gradual loss of the granular layer with progression along hierarchy. In macaque cortex, we found a very strong correlation between myelin map and cytoarchitectural type[4] (Fig. 2a). In human cortex, we examined average expression profiles of genes reported to be preferentially expressed in specific cortical layers[16]. Consistent with trends observed in macaque, we found a positive MMC for granular (L4) layer-specific genes, and negative MMCs for supra- (L1–3) and infra-granular (L5/6) layer-specific genes (Fig. 2b,c). These findings demonstrate that the noninvasive myelin map captures anatomical gradients related to cortical hierarchy in humans and nonhuman primates.

To gain further insight into microcircuit bases of hierarchical specialization, we examined the spatial distributions of markers for distinct inhibitory interneuron cell types. Inhibitory interneuron cell types are biophysically distinct classes which differ in their synaptic connectivity patterns, morphology, electrophysiology, and functional roles[17]. In macaque cortex, we found that densities of parvalbumin- and calretinin-expressing interneurons exhibit positive and negative MMCs, respectively (Fig. 2d). In human cortex, we found highly consistent gradients in the expression profiles for the genes which code for parvalbumin and calretinin (Fig. 2e). Strong hierarchical gradients were observed in transcriptional markers for a number of inhibitory interneuron cell types[17] (Fig. 2f), as well as for composite gene profiles for specific cell types derived from RNA sequencing in individual human neurons[18] (Extended Data Figs. 4). These findings suggest that hierarchical gradients in neuronal cell-type distributions contribute to specialization of cortical microcircuits.

Gradients in the composition of synapses may endow cortical areas with functional specialization needed for diverse computations. One putative microanatomical correlate for the strength of recurrent synaptic excitation in local microcircuits is the number of excitatory synapses on pyramidal neurons, which can be quantified by dendritic spine counts. In macaque cortex, we found a strong negative MMC for basal-dendritic spine counts on pyramidal neurons[19] (Fig. 2g). This suggests a gradient of increasing local

recurrent strength along cortical hierarchy[14]. Distinct subunits of synaptic receptor proteins are expressed differentially across neuronal cell types and produce physiologically diverse synaptic properties. To investigate hierarchical gradients in receptor subunit composition in human cortex, we examined expression profiles of genes that code for various excitatory and inhibitory synaptic receptor subunits (Fig. 2h–j). The gene *GRIN2B*, which codes for a glutamatergic NMDA receptor subunit mediating local synaptic excitation preferentially in association cortex[20], exhibited a strong negative MMC, consistent with the observed macaque spine count gradient. Gene sets coding for neuromodulator receptors also contained hierarchical gradients (Extended Data Fig. 5). The positive and negative MMCs reported in Fig. 2i,j suggest that gradients in local excitatory and inhibitory synaptic machinery contribute to functional specialization of cortical microcircuitry[5,14].

How well does the myelin map capture the transcriptomic architecture of cortex in general? We performed principal component analysis (PCA) to identify the dominant areal patterns underlying gene expression variation (Fig. 3a–e, Extended Data Fig.6). We analyzed categorical sets of genes which are preferentially expressed in human brain, neurons, oligodendrocytes, and synaptic processes[21], and developed a method to assess statistical significance through randomized surrogate data maps that preserve the spatial autocorrelation structure of the myelin map (Extended Data Fig. 7, see Methods). First, we found that myelin map topography is strongly correlated with the dominant axis of

gene expression variation, i.e., the first principal component (PC1) (MMC range: 0.84–0.86; $P < 10^{-4}$ for each set) (Fig. 3b,d). PC1 captures a large fraction of overall gene expression variance (range: 22–28%, more than twice PC2 for each set) (Fig. 3c). PC1 correlated more strongly with the myelin map than with maps of cortical thickness and distance from primary visual cortex (Extended Data Fig. 6d–k). For each gene set, the myelin map captures roughly two-thirds of the variance captured by PC1, which by construction captures the maximum variance for a linear combination of maps (Fig. 3e). The close alignment between myelin map topography and gene expression variance suggests that the dominant axis of human cortical transcriptomic organization relates to hierarchy.

To examine the functional roles of genes with strong hierarchical variation, we tested for their preferential enrichment in gene sets defined by functional and disease ontologies. We found that genes with stronger MMCs are enriched in more functional categories, relative to genes with weaker MMCs, for all functional gene ontologies tested[10,22]: biological processes, cellular components, molecular functions, microRNA binding sites, and drug targets (Fig. 3f). These findings suggest that diverse key cell-biological processes contribute to hierarchical differentiation of cortical microcircuitry. Finally, we examined whether hierarchical expression is a preferential property of genes associated with psychiatric and neurological disorders. The genes *APOE* and *SNCA*, which are strongly linked to Alzheimer's and Parkinson's diseases, respectively[23], exhibit robust negative MMCs,

and therefore higher expression in association cortex (Extended Data Fig. 8). For a systematic examination, we statistically quantified the enrichment of genes with strong hierarchical variation in disease-related gene sets[10], obtained from the DisGeNet database[24]. Genes with strongly negative MMCs were significantly over-represented among multiple disease-related gene sets (Fig. 3g). In particular, sets for schizophrenia, bipolar disorder, autistic disorders, and depressive disorders are enriched with strongly negative MMC genes which are more highly expressed in association cortex. These findings suggest that brain disorders involve differential impacts to areas along the cortical hierarchy.

Taken together, our findings show that cortical hierarchy provides an organizing principle for the transcriptomic architecture of human cortex. Our results support the myelin map as a noninvasive neuroimaging proxy for hierarchical index in the absence of tract-tracing data. Hierarchy, as captured by the myelin map, defines an axis of microcircuit specialization involving synapses and cell types, with relevance to brain disease. Manipulation of hierarchically expressed drug targets would allow regions of sensory or association cortex to be preferentially modulated through pharmacology. Large-scale mapping of the cortical transcriptome at finer spatial resolution will further elucidate the microcircuit basis of hierarchical specialization with laminar[16] and cell-type[12,18] specificity. Furthermore, characterization of the developmental trajectory of hierarchical transcriptomic specialization[25–27] may inform the progression of neurodevelopmental disor-

ders. Our findings add to a growing understanding of how transcriptomic specialization shapes cortical function, including the spatiotemporal structure of intrinsic activity[10,28,29] and anatomical connectivity[11,30]. Hierarchical gradients of microcircuit properties across the human cortex may play key roles in functional specialization across large-scale cortical networks.

Acknowledgements We thank B.D. Fulcher, X.-J. Wang, R. Chaudhuri, and D.C. Glahn for useful discussions. This research was supported by BlackThorn Therapeutics and NIH grants R01MH112746, R01MH108590, and TL1 TR000141.

Author Contributions J.B.B., W.J.M., A.B., A.A. and J.D.M. designed the research. J.B.B., M.D., W.J.E., N.N., and L.J. analyzed the data. J.D.M. supervised the project. J.B.B. and J.D.M. wrote the manuscript and prepared the figures. All authors contributed to editing the manuscript.

Author Information Correspondence and requests for materials should be addressed to J.D.M. (john.murray@yale.edu).

1. Felleman, D. J. & Van Essen, D. C. Distributed hierarchical processing in the primate cerebral cortex. *Cereb Cortex* **1,** 1–47 (1991).
2. Barbas, H & Rempel-Clower, N. Cortical structure predicts the pattern of corticocortical connections. *Cereb Cortex* **7,** 635–646 (1997).
3. Markov, N. T. *et al.* Anatomy of hierarchy: feedforward and feedback pathways in macaque visual cortex. *J Comp Neurol* **522,** 225–59 (2014).
4. Hilgetag, C. C., Medalla, M., Beul, S. F. & Barbas, H. The primate connectome in context: Principles of connections of the cortical visual system. *Neuroimage* **134,** 685–702 (2016).
5. Murray, J. D. *et al.* A hierarchy of intrinsic timescales across primate cortex. *Nat Neurosci* **17,** 1661–3 (2014).
6. Bastos, A. M. *et al.* Visual areas exert feedforward and feedback influences through distinct frequency channels. *Neuron* **85,** 390–401 (2015).
7. Honey, C. J. *et al.* Slow cortical dynamics and the accumulation of information over long timescales. *Neuron* **76,** 423–434 (2012).
8. Margulies, D. S. *et al.* Situating the default-mode network along a principal gradient of macroscale cortical organization. *Proc Natl Acad Sci U S A* **113,** 12574–12579 (2016).

9. Hawrylycz, M. J. *et al.* An anatomically comprehensive atlas of the adult human brain transcriptome. *Nature* **489,** 391–9 (2012).

10. Hawrylycz, M. *et al.* Canonical genetic signatures of the adult human brain. *Nat Neurosci* **18,** 1832–44 (2015).

11. Fulcher, B. D. & Fornito, A. A transcriptional signature of hub connectivity in the mouse connectome. *Proc Natl Acad Sci U S A* **113,** 1435–40 (2016).

12. Lein, E. S., Belgard, T. G., Hawrylycz, M. & Molnár, Z. Transcriptomic perspectives on neocortical structure, development, evolution, and disease. *Annu Rev Neurosci* **40,** 629–652 (2017).

13. Glasser, M. F. & Van Essen, D. C. Mapping human cortical areas in vivo based on myelin content as revealed by T1- and T2-weighted MRI. *J Neurosci* **31,** 11597–616 (2011).

14. Chaudhuri, R., Knoblauch, K., Gariel, M.-A., Kennedy, H. & Wang, X.-J. A large-scale circuit mechanism for hierarchical dynamical processing in the primate cortex. *Neuron* **88,** 419–31 (2015).

15. Wagstyl, K., Ronan, L., Goodyer, I. M. & Fletcher, P. C. Cortical thickness gradients in structural hierarchies. *Neuroimage* **111,** 241–50 (2015).

16. Zeng, H. *et al.* Large-scale cellular-resolution gene profiling in human neocortex reveals species-specific molecular signatures. *Cell* **149,** 483–96 (2012).

17. Markram, H. *et al.* Interneurons of the neocortical inhibitory system. *Nat Rev Neurosci* **5,** 793–807 (2004).

18. Lake, B. B. *et al.* Neuronal subtypes and diversity revealed by single-nucleus RNA sequencing of the human brain. *Science* **352,** 1586–90 (2016).

19. Elston, G. N. Cortex, cognition and the cell: new insights into the pyramidal neuron and prefrontal function. *Cereb Cortex* **13,** 1124–38 (2003).

20. Wang, H., Stradtman 3rd, G. G., Wang, X.-J. & Gao, W.-J. A specialized NMDA receptor function in layer 5 recurrent microcircuitry of the adult rat prefrontal cortex. *Proc Natl Acad Sci U S A* **105,** 16791–16796 (2008).

21. Genovese, G. *et al.* Increased burden of ultra-rare protein-altering variants among 4,877 individuals with schizophrenia. *Nat Neurosci* **19,** 1433–1441 (2016).

22. Chen, J., Bardes, E. E., Aronow, B. J. & Jegga, A. G. ToppGene Suite for gene list enrichment analysis and candidate gene prioritization. *Nucleic Acids Res* **37,** W305–11 (2009).

23. Bras, J. *et al.* Genetic analysis implicates APOE, SNCA and suggests lysosomal dysfunction in the etiology of dementia with Lewy bodies. *Hum Mol Genet* **23,** 6139–46 (2014).

24. Piñero, J. *et al.* DisGeNET: a comprehensive platform integrating information on human disease-associated genes and variants. *Nucleic Acids Res* **45,** D833–D839 (2017).

25. Johnson, M. B. *et al.* Functional and evolutionary insights into human brain development through global transcriptome analysis. *Neuron* **62,** 494–509 (2009).

26. Bakken, T. E. *et al.* A comprehensive transcriptional map of primate brain development. *Nature* **535,** 367–75 (2016).

27. Whitaker, K. J. *et al.* Adolescence is associated with genomically patterned consolidation of the hubs of the human brain connectome. *Proc Natl Acad Sci U S A* **113,** 9105–10 (2016).

28. Wang, G.-Z. *et al.* Correspondence between resting-state activity and brain gene expression. *Neuron* **88,** 659–66 (2015).

29. Krienen, F. M., Yeo, B. T. T., Ge, T., Buckner, R. L. & Sherwood, C. C. Transcriptional profiles of supragranular-enriched genes associate with corticocortical network architecture in the human brain. *Proc Natl Acad Sci U S A* **113,** E469–78 (2016).

30. Richiardi, J. *et al.* Correlated gene expression supports synchronous activity in brain networks. *Science* **348,** 1241–4 (2015).

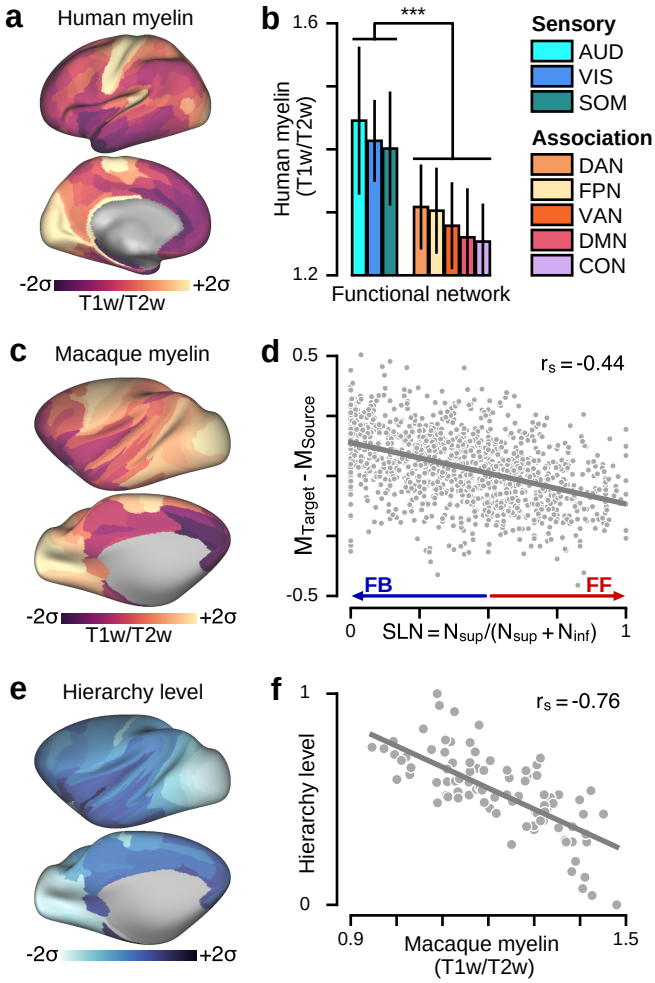

Figure 1: Cortical myelin maps noninvasively capture the hierarchical organization of primate cortex. **a,** The parcellated human myelin map (T1w/T2w MRI signal) in the left cortical hemisphere exhibits high values in primary sensory cortical areas relative to association areas. **b,** Human myelin map values are significantly lower in functionally defined association networks than in sensory networks ($P < 10^{-3}$; Wilcoxon signed-rank test) (see Extended Data Fig. 1c) for network labels). Error bars mark the std. dev. across areas within a network. **c,** The parcellated macaque myelin map topography is similar to that of the human, suggesting that a homologous pattern of intracortical myelination across primate species. **d,** Myelin map variation predicts feedforward (FF) and feedback (FB) interareal projections in macaque cortex, as quantified by the fraction of labeled supragranular layer neurons (SLN) in the source area. High and low SLN correspond to FF and FB projection motifs, respectively. SLN significantly correlates with the difference in myelin map values between target and source areas ($r_s = -0.44$, $P < 10^{-5}$; Spearman rank correlation). **e,** Hierarchy levels across cortical areas are estimated by fitting a generalized linear model to predict SLN from pairwise hierarchical distance. **f,** Hierarchy levels are reliably predicted by the myelin map values in macaque cortex ($r_s = -0.76$, $P < 10^{-5}$), demonstrating that myelin maps provide a noninvasive neuroimaging proxy measure for anatomical hierarchy in primate cortex.

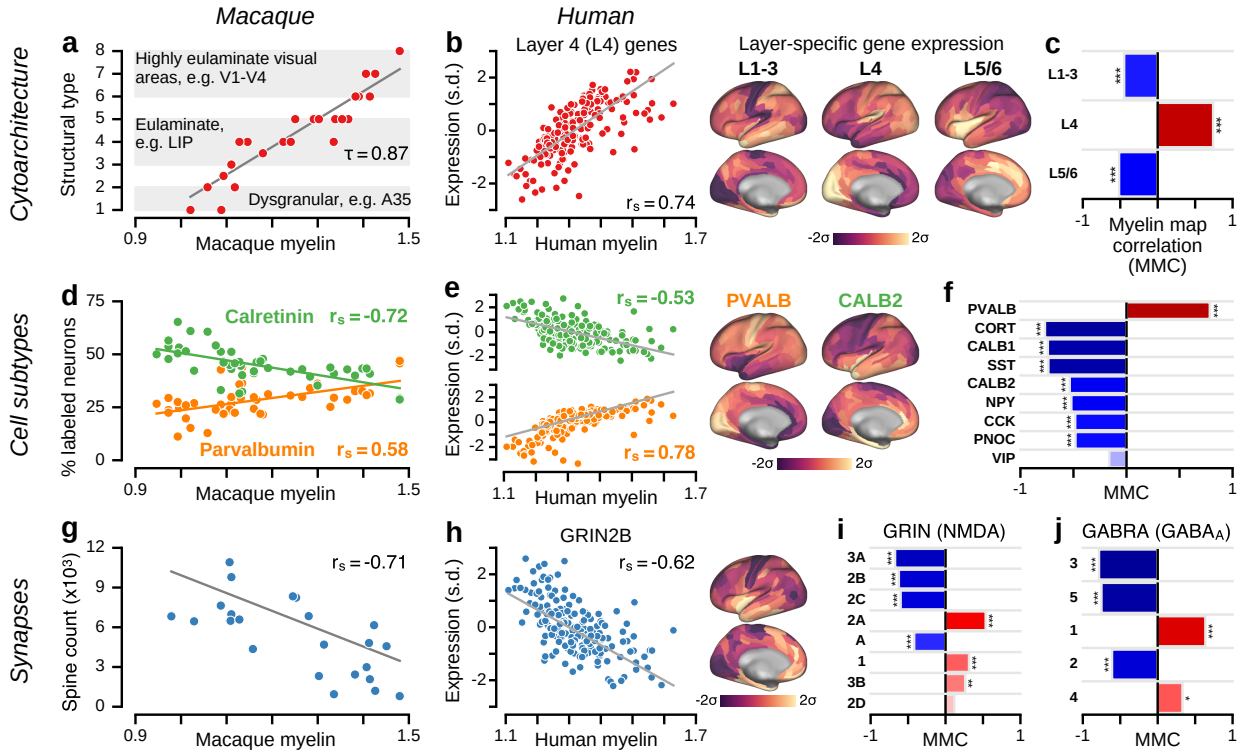

Figure 2: Myelin maps capture specialization of cortical microcircuitry in humans and nonhuman primates, for cytoarchitecture, inhibitory cell types, and synaptic composition. **a,** Cytoarchitectural type is reliably predicted by the myelin map in macaque cortex ($\tau = 0.87$, $P < 10^{-5}$; Kendall's tau correlation coefficient). Cortical areas were classified into one of eight cytoarchitectural types according to laminar thickness, laminar differentiation, and neuronal density. **b,** The average expression map of genes preferentially expressed in human granular layer 4 (L4) is positively correlated with myelin map values ($r_s = 0.74$, $P < 10^{-5}$; Spearman rank correlation), consistent with a more prominent granular L4 in sensory than association cortex. **c,** Average expression maps of laminar-specific genes, which are preferentially expressed in specific cortical layers in humans, show significant myelin map correlations (MMCs). L1-3: supragranular layers 1-3; L5/6: infragranular layers 5 and 6. **d,** The macaque cortical myelin maps capture areal variation in the relative proportions of calretinin- and parvalbumin-positive inhibitory interneurons. **e,** The genes *CALB2* and *PVALB*, which respectively code for calretinin and parvalbumin, exhibit hierarchical gradients in human cortex that are consistent with anatomical gradients in the macaque. **f,** Expression maps of established genes coding for markers of specific inhibitory interneuron cell types exhibit hierarchical gradients across human cortex. **g,** Basal-dendritic spine counts on pyramidal cells are significantly anti-correlated with myelin map values ($r_s = -0.71$, $P < 10^{-4}$). **h,** The gene *GRIN2B*, which codes for the NMDA receptor subunit NR2B, exhibits a negative MMC ($r_s = -0.62$, $P < 10^{-4}$). **i, j,** Expression maps for genes coding for distinct subunits of the excitatory NMDA receptor and inhibitory $\mathrm{GABA_A}$ receptor exhibit both positive and negative hierarchical gradients. For bar plots, statistical significance is calculated through a spatial autoregressive model to account for spatial autocorrelation in maps: *, $P < 10^{-1}$; **, $P < 10^{-2}$; ***, $P < 10^{-3}$.

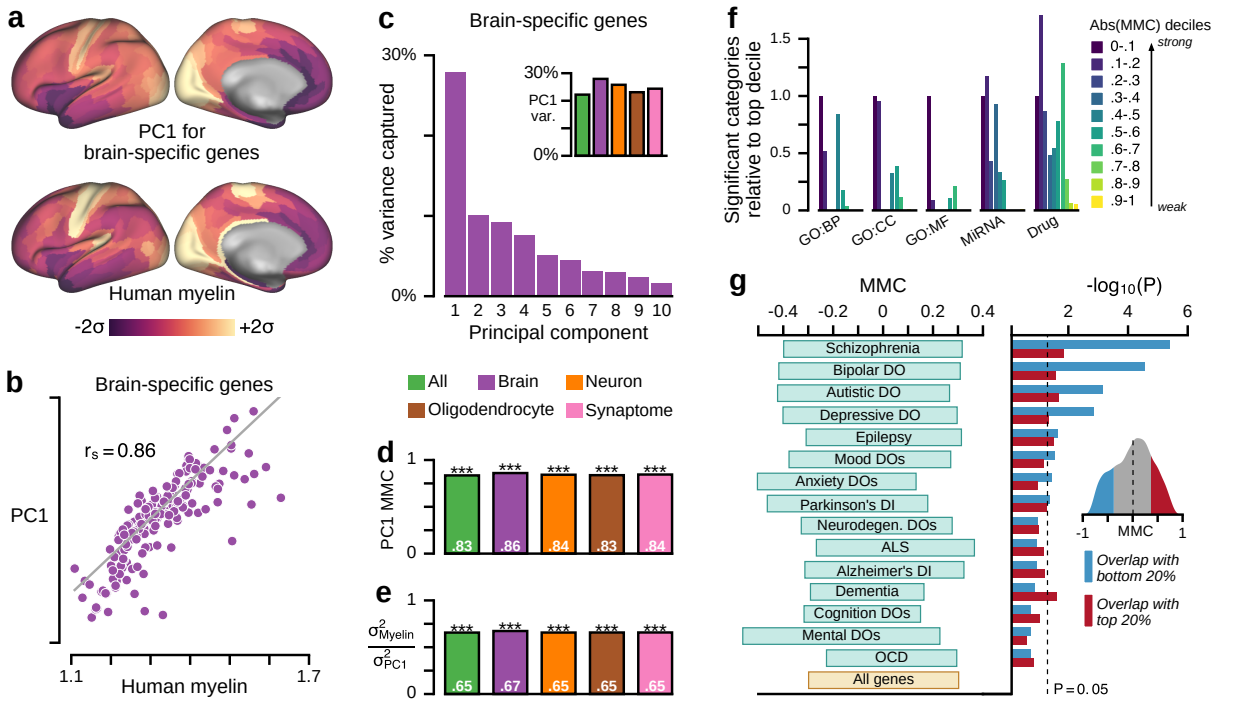

Figure 3: The myelin map captures the dominant spatial axis of gene expression variation across human cortex, as defined by principal component analysis (PCA), and hierarchical variation relates to enrichment in neurobiological function and brain disorders. **a,** The first spatial principal component (PC1), shown here for a set of brain-specific genes, is by definition the spatial map that linearly captures the maximum variation in gene expression. **b,** PC1 for this set is highly correlated with the myelin map (MMC = 0.86; $P < 10^{-4}$). **c,** PC1 captures a large fraction of total gene expression variance. *Inset:* Variance captured by PC1 for five gene sets: all genes in our dataset; genes preferentially expressed in brain relative to other human tissues; genes preferentially expressed in either neurons or oligodendrocytes relative to other brain cell types; and genes related to synaptic processes. **d,** Across all gene sets, PC1 exhibits a highly similar areal topography to the myelin map (MMC range: 0.84–0.86; $P < 10^{-4}$ for each). **e,** The amount of gene expression variance captured by the myelin map (σ^2_{Myelin}) is roughly two-thirds of the theoretical maximum established by PC1 (σ^2_{PC1}). For panels (d,e), statistical significance is calculated through permutation testing with surrogate maps that preserve the spatial autocorrelation structure of the myelin map (see Methods): *, $P < 10^{-1}$; **, $P < 10^{-2}$; ***, $P < 10^{-3}$. **f,** Gene ontology enrichment analysis, using quantiles of absolute MMC. Genes with strong MMCs are overrepresented in functional annotations across multiple gene ontologies (GO). BP, biological process; CC, cellular component; MF, molecular function; MiRNA, microRNA binding site. **g,** Genes with strong negative MMCs are overrepresented in multiple gene sets associated with brain disorders. *Left panel:* Interquartile ranges of MMC for gene sets. *Right panel:* Enrichment is quantified by the hypergeometric test, which assesses the statistical significance of overlap between each gene set and the top (red) or bottom (blue) 20% MMC genes. DO, disorder; DI, disease; ALS, amyotrophic lateral sclerosis; OCD, obsessive-compulsive disorder. *Inset:* Distribution of MMCs across genes. The dotted line marks the mean of the population (0.006).

Methods

Parcellated cortical myelin maps (T1w/T2w). Cortical myelin maps were defined as the ratio of T1- to T2-weighted (T1w/T2w) MRI maps as previously characterized[13,31], using the surface-based CIFTI format[32]. The T1w/Tw2 map has been shown to correlate with grey-matter intracortical myelination and to reflect architectonic boundaries between cortical areas[13,31]. Of note, it may not index myelin content in white matter. The group-averaged ($N = 69$) human myelin map was obtained from the publicly available Conte69 dataset, which was reported previously to study myelin maps[13]. The group-averaged ($N = 334$) cortical thickness map was obtained from the Human Connectome Project (HCP)[33]. Human myelin map values for the left cortical hemisphere were parcellated into 180 areas using the Multi-Modal Parcellation (MMP1.0) from the HCP[32]. Assignment of MMP1.0 parcels to functional networks (Fig. 1b, Extended Data Fig. 1c) was performed through community detection analysis[34] on time-series correlation from the HCP resting-state fMRI dataset.

The group-averaged macaque myelin and thickness maps were obtained from the publicly available BALSA database[35] ($N = 19$) (`https://balsa.wustl.edu/study/show/W336`). Macaque myelin map values for the left cortical hemisphere were parcellated into 91 areas using the M132 parcellation which was used for the anatomical tract-tracing dataset[35]. Geodesic distance between two parcels i and j is calculated as the

average of all pairwise surface-based distances between grayordinate vertices in parcel i and vertices in parcel j.

Anatomical hierarchy levels in macaque. To assess whether macaque cortical myelin maps could reliably capture the laminar-specific interareal projection patterns conventionally used to define anatomical hierarchy, we fit a generalized linear model (GLM) to quantitative laminar projection data, yielding ordinal hierarchy values in 89 cortical areas, following the procedure of ref. [3]. Anatomical tract-tracing data, derived from retrograde tracers, was obtained from the publicly available Core-Nets database (`http://core-nets.org`). Retrograde tracer was injected into a target area i, and the number of labeled neurons in source area j were counted. The fraction of external labeled neurons, $FLNe_{ij}$, is a quantitative measure of connection strength defined as the number of labeled neurons in the source area normalized by the total number of labeled neurons in all external cortical source areas for a given injection[36]. Labeled neurons in the source areas are classified by location in either supragranular or infragranular layers. For a given projection, the proportion of supragranular labeled neurons, SLN_{ij}, is defined as the ratio of N_{supra} to N_{supra} + N_{infra} for neurons labeled in source area j. As feedforward and feedback connections preferentially originate in supragranular and infragranular layers, respectively[1–3], SLN is a quantitative measure of hierarchical distance between two cortical areas[3]: under this paradigm for laminar-specific projection motifs, a

pure feedforward connection from source area j to target area i would originate entirely in the superficial layers, resulting in an SLN of 1. Conversely, a pure feedback projection originating entirely in deep infragranular layers would result in an SLN of 0.

The GLM procedure for fitting hierarchy from SLN data is described in detail in ref. [3]. In brief, the hypothesis that SLN is indicative of hierarchical distance can be expressed as $g(SLN_{ij}) = H_i - H_j$, where H_i corresponds to the hierarchical position of area i, and g is an arbitrary and possibly nonlinear function linking SLN values on the unit interval (0, 1) to their corresponding hierarchical distance. We used a logit link function to map SLN values from the unit interval to the entire real number line following the procedure of ref. [14]. Fitting linear predictors (i.e. hierarchical levels) to logit-transformed SLN values formulates a type of generalized linear model, with maximum likelihood estimation assuming a binomial family probability distribution for the supra- and infragranular neuron counts. To assign more weight to stronger connections during model estimation of hierarchical levels, we also weight each pathway in the model by the negative logarithm of the FLNe value. We clip SLN values to lie in the interval (0.01, 0.99) so the logit-transformed SLN value is well-defined for all pathways used to fit the model. Furthermore, to reduce the impact of noise on model parameter estimation, we only included pathways which contained at least 100 projection neurons when fitting the GLM; we confirmed that results were generally robust to the choice of neuron count threshold.

Maximum likelihood estimation of model parameters was done in the R programming language using the `glm` function. The model-estimated hierarchy levels, invariant under linear transformations, were rescaled to span the unit interval $[0, 1]$. To assess the statistical relationship between myelin map value and hierarchy level, we calculated the Spearman rank correlation between the 89 ordinal hierarchy values and their corresponding parcellated myelin map values (Fig. 1f). For visual clarity in Fig. 1c,d we remove this nonlinear transformation by displaying model-estimated hierarchy levels after applying the inverse-logit (i.e., logistic) transformation. This rescaling preserves the ordering of areas and therefore does not affect the reported Spearman rank correlations.

Macaque anatomical data: cytoarchitectural types, inhibitory interneuron densities, and pyramidal neuron spine counts. To quantify the statistical relationship between myelin map value and categorical cytoarchitectural type (Fig. 2a), we compared myelin map values to structural classification values reported for 29 regions of primate visual cortex, obtained from ref. [4]. To characterize hierarchical distributions of cortical inhibitory interneuron cell types (Fig. 2b), we compiled, from multiple immunohistochemical studies, the relative densities of inhibitory interneurons which are immunoreactive (ir) to the three calcium-binding proteins parvalbumin (PV), calretinin (CR), and calbindin (CB)[37–40]. To characterize hierarchical variation in pyramidal neuron excitatory synaptic connectivity (Fig. 2c), we compiled, from multiple studies by Elston and colleagues[41–46], the number

of spines of basal-dendritic trees of layer-3 pyramidal neurons.

For each of these three analyses, we produced a mapping between the 91 areas in the M132 atlas parcellation, where the myelin map values are calculated, to the architectonic areas reported in these collated studies (Supplementary Table 1). Where the anatomical mapping was not a one-to-one correspondence, we mapped the reported anatomical area onto the set of all M132 parcels with nonzero spatial overlap, and the myelin map value was calculated as the average across these M312 parcels.

Gene expression preprocessing. The Allen Human Brain Atlas (AHBA) is a publicly available transcriptional atlas containing gene expression data, measured with DNA microarrays, that are sampled from hundreds of histologically validated neuroanatomical structures across six normal post-mortem human brains[9]. After no significant interhemispheric transcriptional differences were observed in the first two bilaterally profiled brains[9], the remaining four donor brains were profiled only in the left cortical hemisphere[10]. To construct parcellated group-averaged expression maps, we therefore restricted all analyses to microarray data sampled from the left cortical hemisphere in each of the six brains. Microarray expression data and all accompanying metadata were downloaded from the AHBA (`http://human.brain-map.org`)[9,10]. The raw microarray expression data for each of the six donors includes expression levels of 20,737 genes, profiled by 58,692 microarray probes. These data were preprocessed according to following

procedure:

1. Gene probes without a valid Entrez Gene ID were excluded.

2. Cortical samples exhibiting exceptionally low inter-areal similarity were excluded. We first computed the spatial correlation matrix of expression values between samples using the remaining 48,170 probes, then summed this matrix across all samples. Samples whose similarity measure was more than five standard deviations below the mean across all samples were excluded. At most, this step excluded three samples within a subject.

3. Samples whose annotations did not indicate that they originated in the left hemisphere of the cerebral cortex were excluded. To focus analysis to neocortex, we also excluded samples taken from cortical structures that are cytoarchitecturally similar to the hippocampus, including the rhinal sulcus, piriform cortex, parahippocampal gyrus, and the hippocampal formation.

4. The remaining cortical samples were mapped from volumetric space onto a two dimensional cortical surface by minimizing the pairwise 3D Euclidean distance between the stereotaxic MNI coordinates reported for each sample, and each grayordinate vertex in the group-averaged surface mesh of the midthickness map in the Conte69 brain atlas. Cortical samples whose Euclidean distance to the nearest surface vertex was more than two standard deviations above the mean distance computed across all sam-

ples were excluded (excluding between 4 and 13 samples per subject). An average of 203 $\pm$ 32 samples per subject, yielding 1219 total samples across all six subjects, remained at this stage.

5. Expression profiles for samples mapped onto the same surface vertex were averaged. Then expression profiles for each remaining sample were z-scored across gene probes.

6. Expression profiles for each of the 180 unilateral parcels in the HCP's MMP1.0 cortical parcellation[32] were computed in one of the two following ways. (I) For parcels which had at least one sample mapped directly onto one of their constituent surface vertices, parcellated expression values were computed by averaging expression levels across all samples mapped onto the parcel. (II) For parcels which had no samples mapped onto any of their constituent vertices, we first created densely interpolated expression maps, in which each surface vertex was assigned the expression level associated with the most proximal surface vertex onto which a sample had been mapped (i.e., a Voronoi diagram), determined using surface-based geodesic distance along the cortical surface; the average of expression levels across parcels' constituent vertices was then computed to obtain parcellated expression values.

7. A coverage score was also assigned to each gene probe, defined as the fraction of 180 parcels that had at least one sample mapped directly onto one of its constituent surface vertices. Probes with coverage below 0.4 (i.e., probes for which fewer than 72 of the

379 180 parcels contained samples) were excluded.

380 8. For each gene profiled by multiple gene probes, we selected and used the expression
381 profile of a single representative probe. If two probes were available, we selected the
382 probe with maximum gene expression variance across sampled cortical structures, in
383 order to more reliably capture spatial patterns of areal heterogeneity. If three or more
384 probes were available, we selected a probe using a procedure similar to the one de-
385 scribed in step 2: we computed a correlation matrix of parcellated gene expression
386 values across the available gene probes, summed the resultant matrix along one of its
387 dimensions to obtain a quantitative similarity measure for each probe, relative to the
388 other gene probes, and selected the probe with the highest similarity measure, as it is
389 most highly representative among all available gene probes.

390 9. Each subject-level gene expression profile was z-scored before we computed group-
391 level expression profiles, which were obtained by computing the mean across subjects
392 which were assigned a probe for that gene. Genes were excluded if fewer than four
393 subjects were assigned a probe. Finally, group-level expression profiles were z-scored
394 across areas for each gene.

395 These steps yielded group-averaged expression values for 16,040 genes across 180 cortical
396 areas, which were used for all analyses reported here. The myelin map correlation (MMC)
397 for each gene is reported in Supplementary Table 2.

Categorical gene sets. We conducted analyses on biologically and physiologically meaningful gene sets extracted from existing databases and neuroscientific literature, reported below (Supplementary Table 2):

1. **Brain-specific.** Genes with expression specific to human brain tissue, relative to other tissues, were obtained from supplementary data set 1 of ref. [47]. Following ref. [21], brain-specific genes were selected for which expression in brain tissue was four times higher than the median expression across all 27 different tissues.

2. **Neuron- and oligodendrocyte-specific.** Brain genes with expression specific to neurons or oligodendrocytes, relative to other central nervous system (CNS) cell types, were obtained from supplementary data set S3b of ref. [48]. Following ref. [21], neuron-specific genes were selected for which log-expression in neurons of P7n cell type in the mouse was 0.5 greater than the median log-expression across 11 CNS cell types.

3. **Synaptome.** Four synaptic gene sets encoding proteins in the presynaptic nerve terminal, presynaptic active zone, synaptic vesicles, and postsynaptic density, were obtained from SynaptomeDB, an ontology-based database of genes in the human synaptome[49].

4. **Neuron subtype-specific.** Gene sets representing distinct classes of neuronal subtypes were obtained from ref. [18], in which clustering and classification analyses

yielded 16 distinct neuron subtypes, on the basis of differential gene expression measured by RNA sequencing from single neurons in human cortex. The fraction of positive values using exon-only derived transcripts per million (TPM) associated with each subtype-specific gene were obtained from supplementary table S5; within each neuronal subtype cluster, the TPM values for the cluster genes were normalized and used to create a weighted gene expression profile representative of each subtype's spatial topography (Extended Data Fig. 4).

5. **Layer-specific.** Sets of laminar-specific genes localized to different layers of human neocortex were obtained from supplementary table S2 of ref. [16]. Genes were broadly grouped into sets representative of supragranular (L1–3), granular (L4), and infragranular (L5/6) layers.

Spatial autoregressive modeling. Significance values as indicated by the number of stars reported on barplots for myelin map correlations were corrected to account for spatial autocorrelation structure in parcellated myelin map and gene expression values. Because physical quantities like cortical myelination and gene expression must vary smoothly and continuously in space, measurements recorded from proximal cortical areas tend to be more similar than measurements recorded from distal areas of cortex. This departure from the assumption of independent observations biases calculations of statistical significance. To model this spatial autocorrelation, we used a spatial lag model (SLM)

commonly applied in the spatial econometrics literature[50], of the form $y = \rho W y + X\beta + \nu$, where W is a weight matrix implicitly specifying the form of spatial structure in the data, and ν is normally distributed.

To implement a spatial lag model in the python programming language, we used the maximum likelihood estimation routine defined in the Python Spatial Analysis Library (*pysal*)[51]. We first determined the surface-based spatial separation between each pair of cortical parcels by computing the mean of the pairwise distances between a vertex in parcel i and a vertex in parcel j, from which we constructed a pairwise parcel distance matrix, D.

Similarity of gene expression profiles was well-approximated by an exponential decaying spatial autocorrelation function (Extended Data Fig. 7), as was found in mouse cortex[11]. We fitted the correlation of gene expression profiles between two areas with the exponential function $\mathrm{Corr}(x_i, x_j) \sim \exp(-D_{ij}/d_0)$, where x_i and x_j are vectors containing the parcellated gene expression values at parcels i and j, D_{ij} is the geodesic distance between the parcels, and d_0 is the characteristic spatial scale of autocorrelation. We empirically determined d_0 by first constructing the pairwise gene co-expression matrix $C_{ij} = \mathrm{Corr}(x_i, x_x)$, where x_i and x_j are vectors containing the parcellated gene expression values at parcels i and j. We then fit the free parameter d_0 using ordinary least squares (OLS) regression on the off-diagonal (upper-triangular) elements of the gene co-expression and

parcel distance matrices, so as to minimize the sum-of-squared-residuals between empirical and model-estimated gene co-expression values over all pairs of cortical parcels, $S = \sum_{i>j} r_{ij}^2 = \sum_{i>j} [C_{ij} - \exp(-D_{ij}/d_0)]^2$. This empirical fit was performed on a set of brain-specific genes. Using the OLS estimate of the spatial autocorrelation scale from the fit to the empirical gene expression data, we calculated the elements of the spatial weight matrix, $W_{ij} = \exp(-D_{ij}/d_0)$. Finally, we fit the SLM to parcellated gene expression profiles, using the maximum likelihood estimator routine (`pysal.spreg.ml_lag.ML_Lag`) in *pysal*. P-values indicated by the number of stars in the bar plots of myelin map correlation correspond to p-values for model parameter β defined above.

Of note, spatial autoregressive model parameters do not have the same interpretation as they do in OLS regression. The parameter β reflects the direct (i.e. local) impact on the dependent variable y due to a unit change in the independent variable x. In addition, because of the underlying spatial structure, the direct impact of x_i on y_i results in an indirect effect of y_i on neighboring y_j. Therefore β cannot be interpreted as a corrected, global correlation coefficient, and we restrict our use of the SLM to correcting for the biasing effect of spatially autocorrelated samples on reported significance values.

Theil-Sen estimator. Trend lines in figures are calculated by the Theil-Sen estimator, which is a nonparametric estimator of linear slope, based on Kendall's tau rank correlation, that is insensitive to the underlying distribution and robust to statistical outliers[52].

It is defined as the median of the set of slopes computed between all pairs of points.

Principal components analysis. We used principal component analysis (PCA) to identify the dominant modes of spatial variation in the transcriptional profiles of gene expression in the human cortex. For a set of N genes, each with group-averaged expression values for P cortical parcels, we constructed a gene expression matrix $\mathbf{G}$ with one row for each cortical parcel and one column for each unique gene (i.e. with dimensions $P \times N$). The $P \times P$ spatial covariance matrix $\mathbf{C}$ was constructed by computing the covariance between vectors of gene expression values for each pair of cortical parcels: $C_{ij} = \text{Cov}(G_i, G_j)$, where G_i is the i-th row in the matrix $\mathbf{G}$, corresponding to the vector of N gene expression values for the i-th cortical parcel. Eigen-decomposition is performed on the spatial covariance matrix to obtain the matrix eigenvectors (i.e., the principal components, PCs) and their corresponding eigenvalues, which are the amount of variance captured by the corresponding PC. To enumerate each principal component, eigenvalues are ranked in descending order of absolute magnitude, with larger magnitudes indicating a greater proportion of the total variance captured by the associated PC (i.e., the associated mode of spatial covariation). PCA therefore allows for simultaneous identification of spatial patterns of covariation and quantification of the extent to which these spatial modes capture variance in cortical gene expression profiles.

To quantify the overlap of these spatial PCs with the cortical myelin map vector, we

compute the Spearman rank correlation coefficient between each P-dimensional PC and the P-dimensional vector of myelin map values for each cortical parcel. We can quantify the amount of gene expression variance that is captured along any given spatial map, such as the myelin map (Fig. 3e, Extended Data Fig. 6g,k). From the spatial covariance matrix $\mathbf{C}$, the variance captured along a unit-length vector $\mathbf{a}$, here a demeaned and normalized map, is given by $\mathbf{a}^\top \mathbf{C}\mathbf{a}$.

Surrogate data generation. To nonparametrically determine significance values in our PCA results, in Fig. 3 and Extended Data Fig. 6, we generated surrogate maps with a spatial autocorrelation structure matched to the empirical data (Extended Data Fig. 7b). Parameters characterizing the empirical spatial autocorrelation were determined numerically for the cortical myelin map, cortical thickness map, and the map of surface-based geodesic distance from area V1; in each case, we fit the data using a spatial lag model of the form $\mathbf{y} = \rho\mathbf{W}\mathbf{y}$, where $\mathbf{y}$ is a vector of mean-subtracted map values. $\mathbf{W}$ is the weight matrix with zero diagonal and off-diagonal elements $W_{ij} = \exp(-D_{ij}/d_0)$, where D_{ij} is the surface-based geodesic distance between cortical areas i and j. Two free parameters ρ and d_0 are estimated by minimizing the residual sum-of-squares[50]. Using best-fit parameter values $\hat{\rho}$ and $\hat{d}_0$, surrogate maps $\mathbf{y}_{\text{surr}}$ are generated according to $\mathbf{y}_{\text{surr}} = \left(\mathbb{I} - \hat{\rho}\mathbf{W}[\hat{d}_0]\right)^{-1}\mathbf{u}$, where $\mathbf{u} \sim \mathcal{N}(0, 1)$. From these surrogate maps we construct null distributions for the appropriate statistics, and report significance values as the proportion of samples in the null

512 distribution whose absolute value is equal to or greater than the absolute value of the test
513 statistic.

514 **Functional enrichment analyses.** Functional enrichments were determined using the
515 ToppGene (`https://toppgene.cchmc.org/`) web portal[22], including gene ontology
516 annotations (biological process, cellular component, and molecular function); microRNA
517 targets (from all sources indicated on https://toppgene.cchmc.org/navigation/database.jsp);
518 and drug annotations (from DrugBank, Comparative Toxicogenomics Database, includ-
519 ing marker and therapeutic, and Broad Institute CMAP). Significant genes in each cate-
520 gory were identified using the ToppFun utility. Disease annotations were determined us-
521 ing curated disease gene associations in the DisGeNet database[24] (`http://www.disgenet.`
522 `org/web/DisGeNET/menu/home`). Hypergeometric testing was used to determine sig-
523 nificant over-representation of brain-related disease genes in the top and bottom gene
524 quintiles (20%, 3208 genes) ranked by myelin map correlation, following ref. [10].

31. Glasser, M. F., Goyal, M. S., Preuss, T. M., Raichle, M. E. & Van Essen, D. C. Trends and properties of human cerebral cortex: correlations with cortical myelin content. *Neuroimage* **93 Pt 2,** 165–75 (2014).

32. Glasser, M. F. *et al.* A multi-modal parcellation of human cerebral cortex. *Nature* **536,** 171–8 (2016).

33. Van Essen, D. C. *et al.* The WU-Minn Human Connectome Project: an overview. *Neuroimage* **80,** 62–79 (2013).

34. Ito, T. *et al.* Cognitive task information is transferred between brain regions via resting-state network topology. *bioRxiv.* <https://www.biorxiv.org/content/early/2017/08/02/101782> (2017).

35. Donahue, C. J. *et al.* Using diffusion tractography to predict cortical connection strength and distance: a quantitative comparison with tracers in the monkey. *J Neurosci* **36,** 6758–70 (2016).

36. Markov, N. T. *et al.* A weighted and directed interareal connectivity matrix for macaque cerebral cortex. *Cereb Cortex* (2012).

37. Condé, F, Lund, J. S., Jacobowitz, D. M., Baimbridge, K. G. & Lewis, D. A. Local circuit neurons immunoreactive for calretinin, calbindin D-28k or parvalbumin in monkey prefrontal cortex: distribution and morphology. *J Comp Neurol* **341,** 95–116 (1994).

38. Gabbott, P. L. & Bacon, S. J. Local circuit neurons in the medial prefrontal cortex (areas 24a,b,c, 25 and 32) in the monkey: II. Quantitative areal and laminar distributions. *J Comp Neurol* **364,** 609–36 (1996).

39. Kondo, H, Tanaka, K, Hashikawa, T & Jones, E. G. Neurochemical gradients along monkey sensory cortical pathways: calbindin-immunoreactive pyramidal neurons in layers II and III. *Eur J Neurosci* **11,** 4197–203 (1999).

40. Dombrowski, S. M., Hilgetag, C. C. & Barbas, H. Quantitative architecture distinguishes prefrontal cortical systems in the rhesus monkey. *Cereb Cortex* **11,** 975–88 (2001).

41. Elston, G. N. & Rosa, M. G. The occipitoparietal pathway of the macaque monkey: comparison of pyramidal cell morphology in layer III of functionally related cortical visual areas. *Cereb Cortex* **7,** 432–52 (1997).

42. Elston, G. N. & Rosa, M. G. Morphological variation of layer III pyramidal neurones in the occipitotemporal pathway of the macaque monkey visual cortex. *Cereb Cortex* **8,** 278–94 (1998).

43. Elston, G. N., Tweedale, R & Rosa, M. G. Cortical integration in the visual system of the macaque monkey: large-scale morphological differences in the pyramidal neurons in the occipital, parietal and temporal lobes. *Proc Biol Sci* **266,** 1367–74 (1999).

44. Elston, G. N. & Rockland, K. S. The pyramidal cell of the sensorimotor cortex of the macaque monkey: phenotypic variation. *Cereb Cortex* **12,** 1071–8 (2002).

564 45. Elston, G. N., Benavides-Piccione, R. & Defelipe, J. A study of pyramidal cell structure in the cingulate cortex of the macaque monkey with comparative notes on inferotemporal and primary visual cortex. *Cereb Cortex* **15,** 64–73 (2005).

567 46. Elston, G. N., Oga, T., Okamoto, T. & Fujita, I. Spinogenesis and Pruning in the Anterior Ventral Inferotemporal Cortex of the Macaque Monkey: An Intracellular Injection Study of Layer III Pyramidal Cells. *Front Neuroanat* **5,** 42 (2011).

570 47. Fagerberg, L. *et al.* Analysis of the human tissue-specific expression by genome-wide integration of transcriptomics and antibody-based proteomics. *Mol Cell Proteomics* **13,** 397–406 (2014).

573 48. Cahoy, J. D. *et al.* A transcriptome database for astrocytes, neurons, and oligodendrocytes: a new resource for understanding brain development and function. *J Neurosci* **28,** 264–78 (2008).

576 49. Pirooznia, M. *et al.* SynaptomeDB: an ontology-based knowledgebase for synaptic genes. *Bioinformatics* **28,** 897–9 (2012).

578 50. Anselin, L. in *A companion to theoretical econometrics* (ed Baltagi, B. H.) 310–330 (Blackwell, Malden, Mass., 2001).

580 51. Fischer, M. M. & Getis, A. *Handbook of applied spatial analysis: software tools, methods and applications* (Springer, Berlin, 2010).

582 52. Sen, P. K. Estimates of the regression coefficient based on Kendall's tau. *Journal of the American Statistical Association* **63,** 1379–1389 (1968).

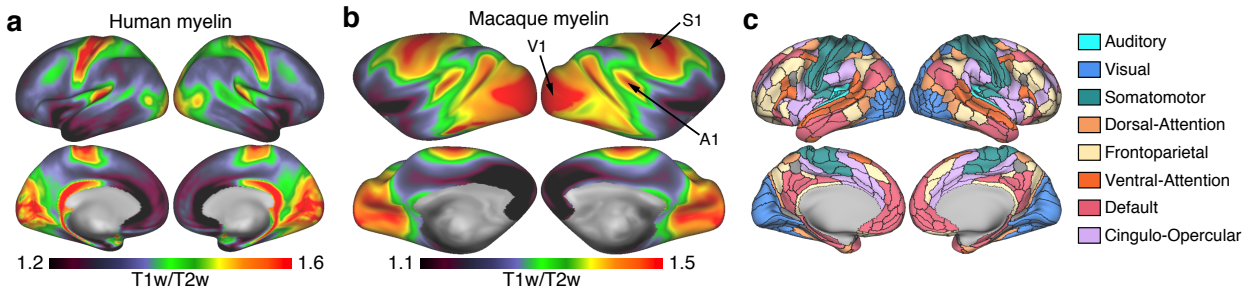

Extended Data Figure 1: Cortical myelin maps exhibit inter-species homology and inter-hemispheric symmetry. **a,** Unparcellated bilateral myelin map (T1w/T2w) in human cortex visualized on an inflated cortical surface. **b,** Unparcellated bilateral myelin map (T1w/T2w) in macaque cortex visualized on an inflated cortical surface. Primary sensory areas (visual, V1; somatosensory, S1; auditory, A1) exhibit high myelin map values, as do their homologues in human cortex. **c,** Functional networks derived from resting-state functional connectivity from the Human Connectome Project (HCP). Cortical areas are parcellated using the HCP multi-modal parcellation (MMP1.0). We assigned each region to a functional network using a community detection method applied to resting-state fMRI data from the HCP, and designated functional labels to networks, including three sensory and five association, that align with previously reported functional networks (with abbreviations labeled in Fig. 1b): Auditory (AUD), Visual (VIS), Somatomotor (SOM), Dorsal Attention (DAN), Frontoparietal (FPN), Ventral Attention (VAN), Default (DMN), and Cingulo-Opercular (CON).

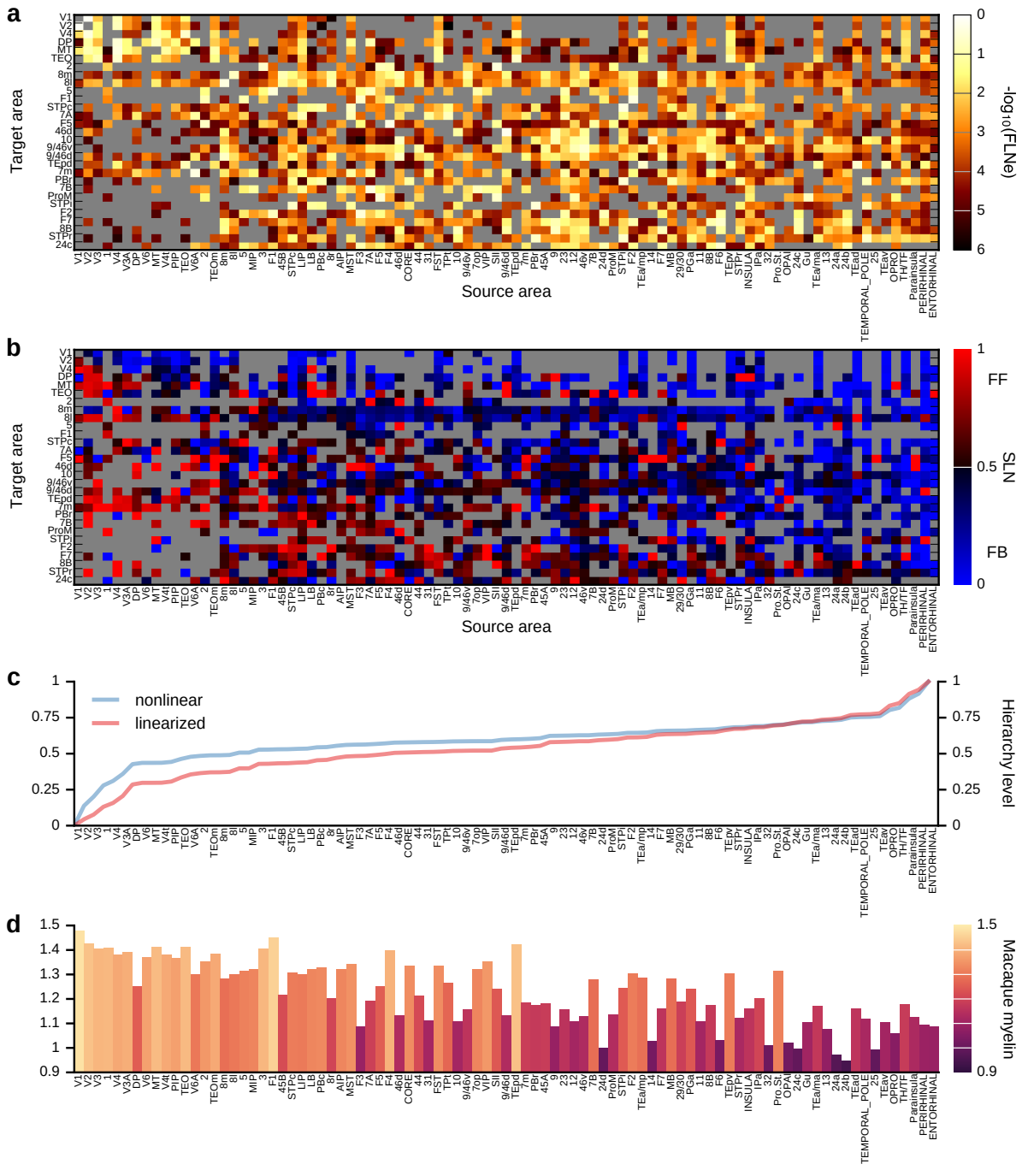

Extended Data Figure 2: [Caption on next page]

Extended Data Figure 2: Anatomical cortical hierarchy derived from laminar-specific interareal projections. **a,** Fraction of external labeled neurons ($FLNe$). Target area i is injected with a retrograde tracer that labels neurons in many source areas; the $FLNe$ in source area j is then defined as the fraction of all external labeled neurons terminating in area i that originated in source area j. Each row of the FLN matrix is therefore normalized to 1. Measurements which yielded no labeled neurons are marked in grey. **b,** Fraction of supragranular layer neurons (SLN), defined as the fraction of neurons in an interareal projection (to target area i from source area j) originating in supragranular layers. An SLN of 1 indicates that all labeled projection neurons were of supragranular origin, reflecting a pure feedforward connection; an SLN of 0 indicates that all projection neurons originated in deep infragranular layers, reflecting a pure feedback connection. Measurements which yielded no labeled neurons are marked in grey. **c,** Model-estimated hierarchy values for 89 cortical regions. The blue line indicates hierarchy levels estimated by the model after shifting and re-scaling them to lie on the unit interval. The red indicates hierarchy values passed through a logistic function to remove the nonlinearity introduced by the logit link function in the GLM fitting procedure. The monotonicity of this transformation preserves the order of the cortical regions and therefore does not affect the Spearman rank correlations reported in the main text. **d,** Myelin map values for 89 cortical regions.

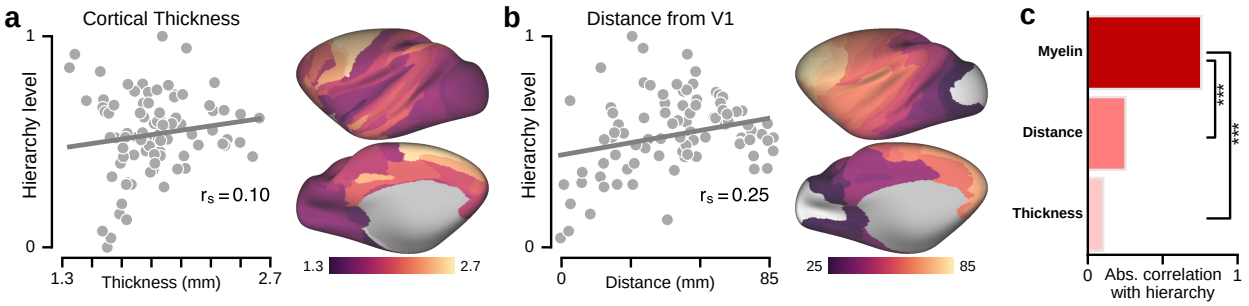

Extended Data Figure 3: Hierarchy in macaque cortex is better captured by the myelin map (T1w/T2w) than by other candidate proxy measures derived from structural MRI. **a,** Correlation between hierarchy and cortical thickness. **b,** Correlation between hierarchy and geodesic distance from primary visual cortex (V1). **c,** Comparison of hierarchy correlation values for the myelin map, thickness map, and distance from V1. The myelin map is much more strongly correlated with hierarchy than the other two maps ($P < 10^{-3}$). Statistical significance is calculated by a test of the difference between dependent correlations: $P < 10^{-1}$; **, $P < 10^{-2}$; ***, $P < 10^{-3}$.

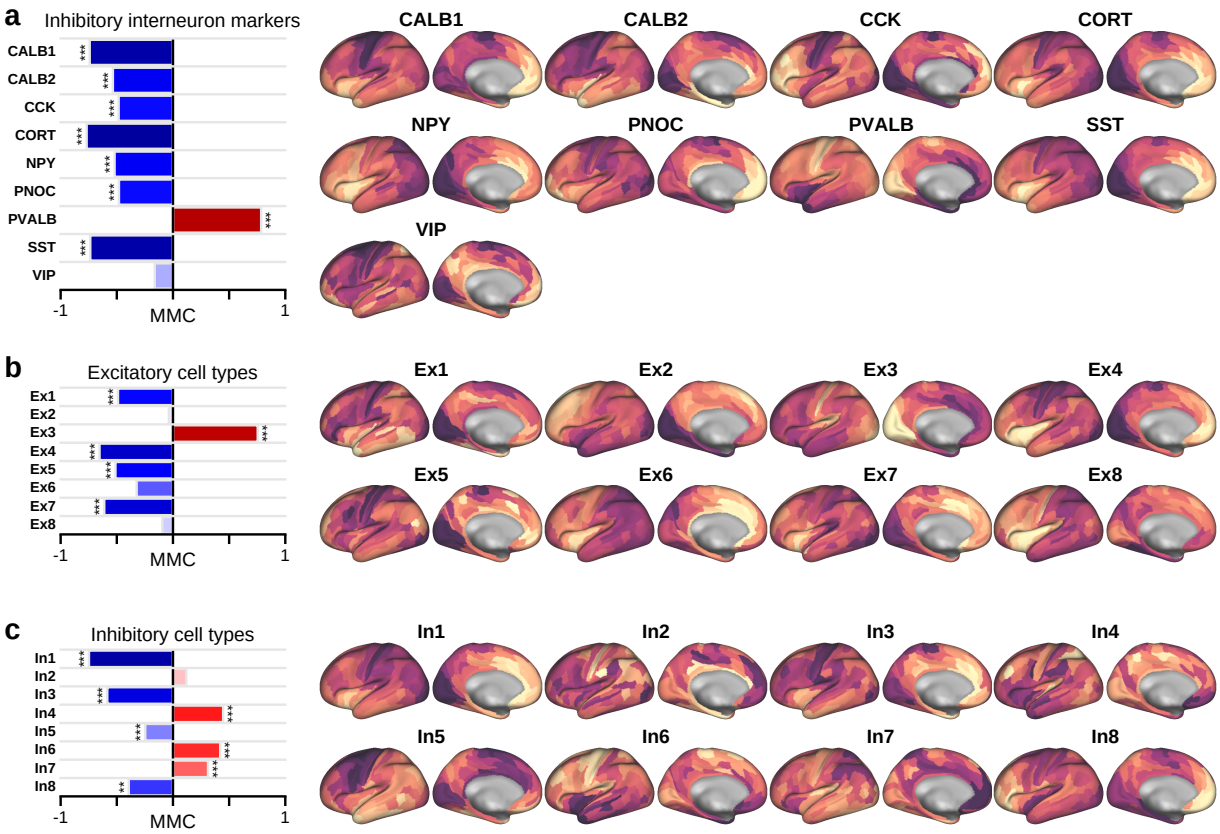

Extended Data Figure 4: Expression maps and MMCs for genes that code for markers of distinct inhibitory interneuron cell types, and for weighted profiles characteristic of distinct neuronal cell types derived from single-cell RNA sequencing of human cortical neurons. **a,** Markers for inhibitory interneuron cell types. **b,** Weighted gene sets for excitatory neuronal cell types, derived from single-cell RNA sequencing. **c,** Weighted gene sets for inhibitory neuronal cell types, derived from single-cell RNA sequencing.

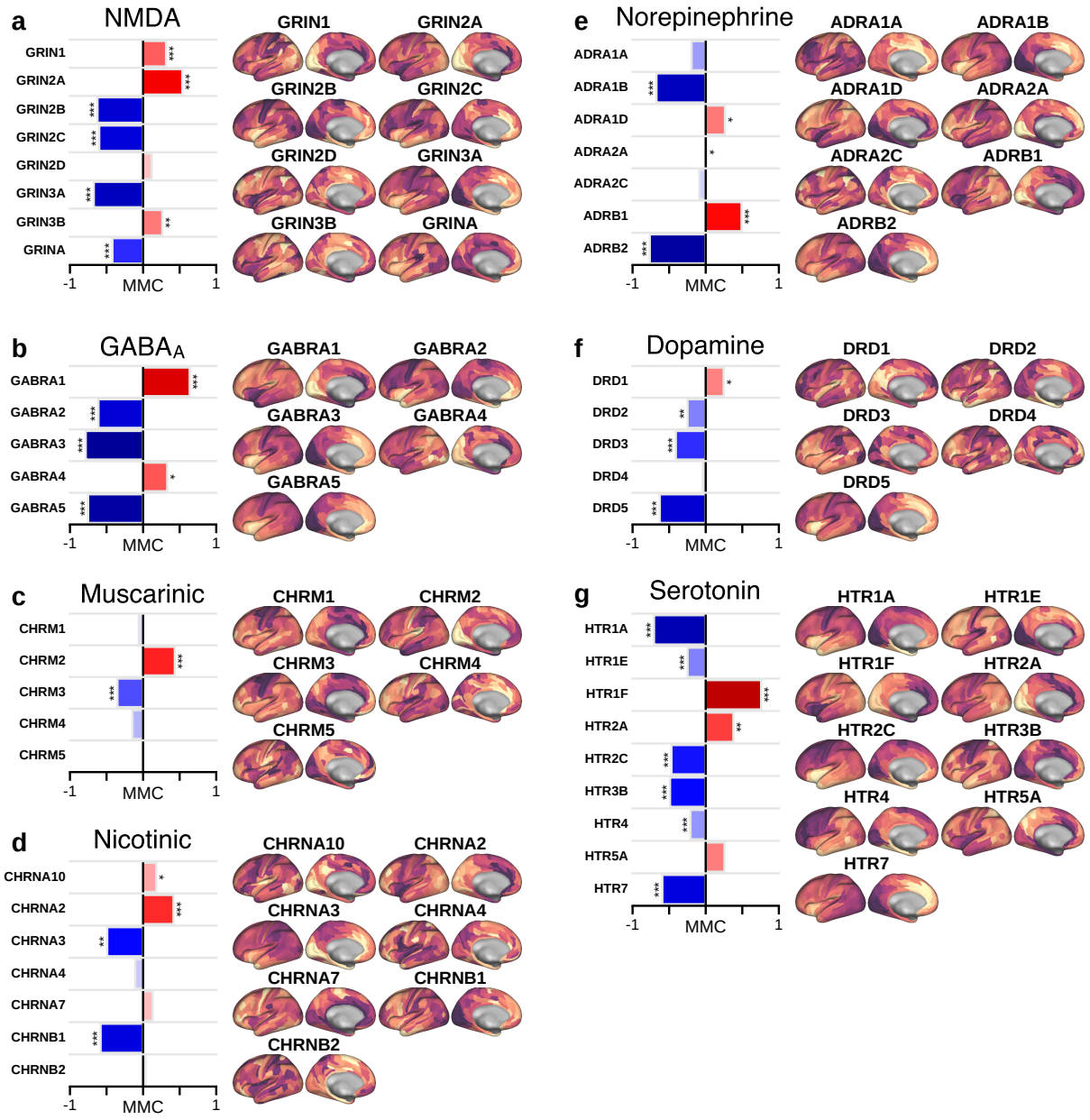

Extended Data Figure 5: Expression maps and MMCs for genes coding for synaptic receptor subunits and neuromodulator receptors. **a,** NMDA receptor subunits. **b,** $\mathrm{GABA_A}$ receptor subunits. **c,** Muscarinic acetylcholine receptors (CHRM). **d,** Nicotinic acetylcholine receptors (CHRN). **e,** Norepinephrine receptors (ADR). **f,** Dopamine receptors (DRD). **g,** Serotonin receptors (HTR).

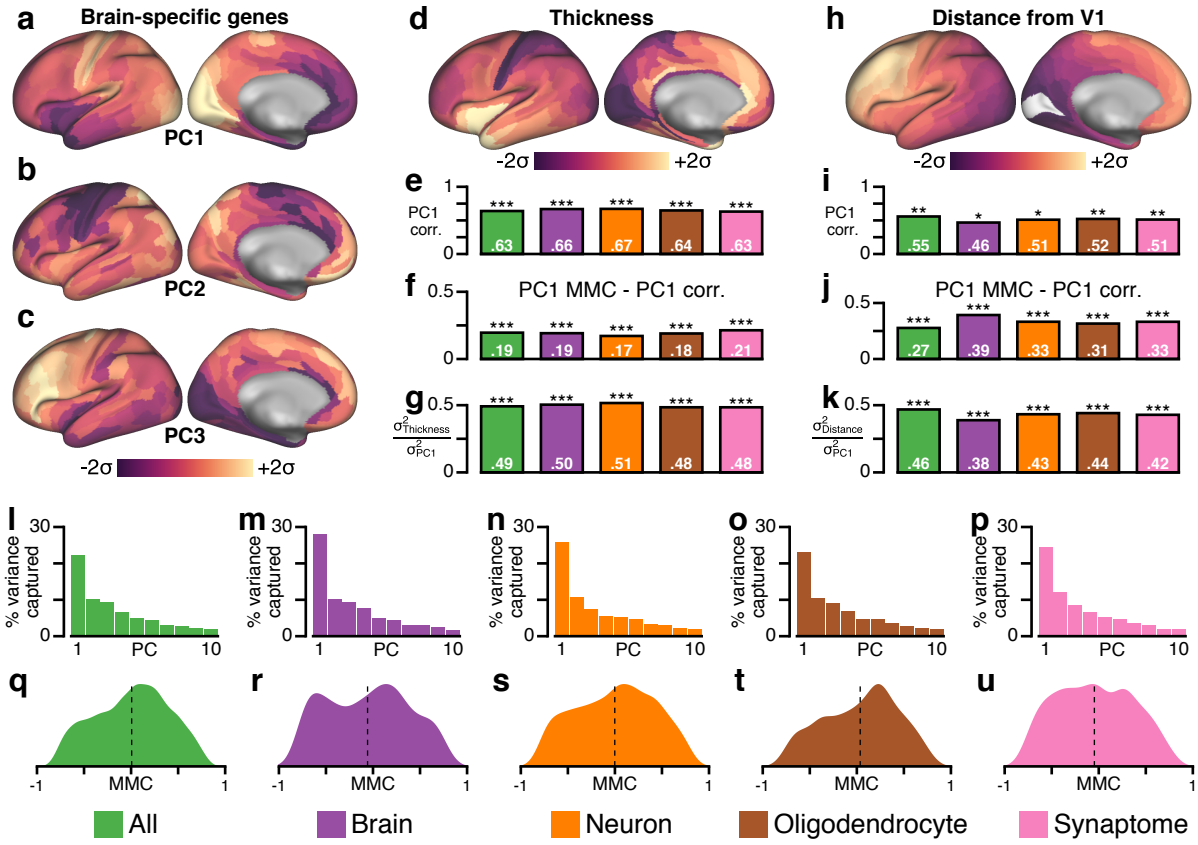

Extended Data Figure 6: Principal component analysis (PCA) shows that the dominant mode of gene expression (PC1) is better captured by the myelin map than by other candidate proxies. **a–c,** The first three PCs for brain-specific genes. **d,** The parcellated map of human cortical thickness. **e,** The Spearman rank correlation between the thickness map and PC1 for five gene sets. **f,** The difference in correlation with PC1 between the thickness map and the myelin map, i.e., $(r_s(\text{Myelin}, \text{PC1}) - r_s(\text{Thickness}, \text{PC1}))$. Positive values indicate that the myelin map is more strongly correlated with PC1 than is the thickness map. Statistical significance is calculated by a test of the difference between dependent correlations ($P < 10^{-1}$; **, $P < 10^{-2}$; ***, $P < 10^{-3}$). **g,** Amount of gene expression variance captured by the thickness map, relative to PC1. **h,** The parcellated map of geodesic distance from primary visual cortical area V1. **i,** The Spearman rank correlation between the V1 distance map and PC1. **j,** The difference in correlation with PC1 between the V1 distance map and the myelin map, i.e., $(r_s(\text{Myelin}, \text{PC1}) - r_s(\text{Distance}, \text{PC1}))$. The myelin map is more strongly correlated with PC1 than is the V1 distance map. **k,** Amount of gene expression variance captured by the thickness map, relative to PC1. **l–p,** Percentage of gene expression variance captured by the top 10 PCs, out of 179 total PCs. For all five gene sets, PC1 captures between 22% and 28% of the variance, which is more than twice the amount captured by PC2. **q–u,** Distribution of myelin map correlations (MMCs) across five gene sets. Dashed lines mark the mean of the distribution. For all five gene sets, the distributions are broad, containing large fractions of strong positive and negative MMCs, and centered near zero, with a range of means $(-0.06, +0.04)$.

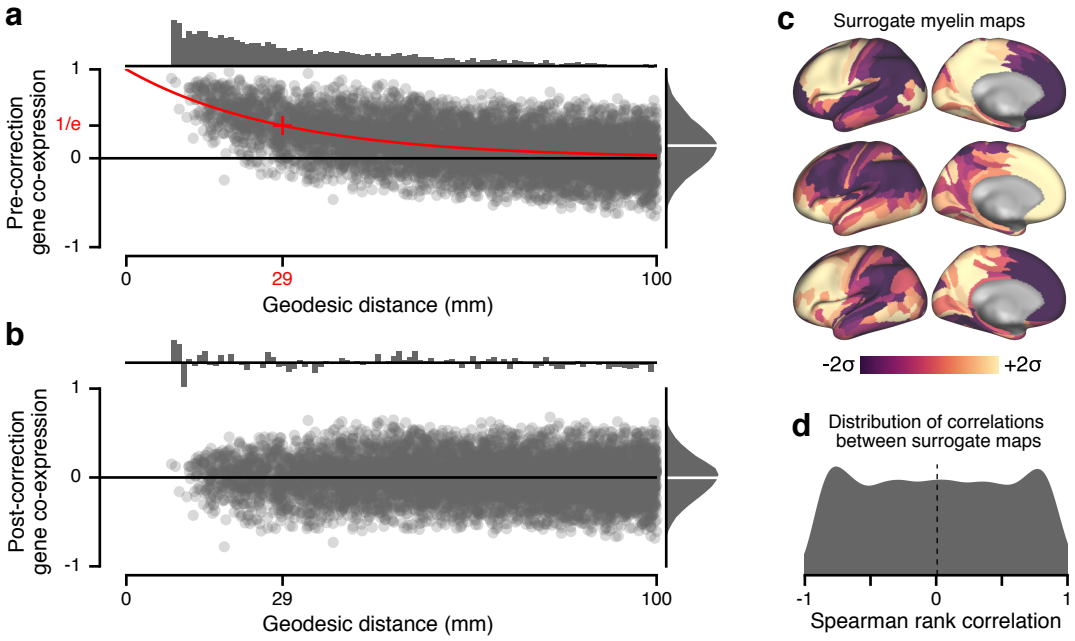

Extended Data Figure 7: Autocorrelation structure in gene expression and myelin maps. **a,** Spatial autocorrelation structure in the parcellated cortical gene expression data is well-approximated by a decaying exponential. Gene co-expression is defined as the pairwise Spearman rank correlation between cortical parcels' gene expression values, here for the brain-specific gene set. Proximal cortical parcels exhibit more similar gene expression values compared to distal parcels. All pairs of parcels with geodesic distance less than 100 mm were used to fit the characteristic scale of spatial autocorrelation, illustrated in red (i.e., $\exp(-d/d_0)$), where d is geodesic distance and $d_0 = 29$ mm. Each data point corresponds to the co-expression of a pair of cortical parcels. *Top*: Mean co-expression value as a function of geodesic distance bin. **b,** Gene co-expression values after correcting for spatial autocorrelation structure by subtraction of the fitted exponential decay. After correction, the mean co-expression value is near zero across all geodesic distance bins. **c,** Example randomized surrogate maps with spatial autocorrelation structure matched to the cortical myelin map (see Methods). Autocorrelation structure-preserving surrogate myelin maps are used for nonparametric calculation of statistical significance for PCA results in Figs. 3 and 6. **d,** Distribution of pairwise Spearman rank correlations between pairs of surrogate myelin maps.

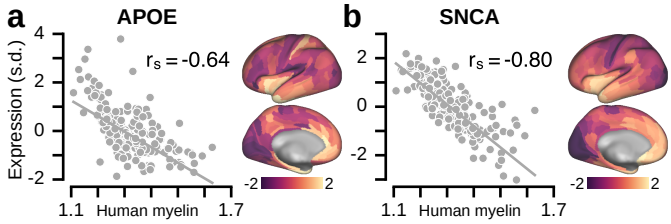

Extended Data Figure 8: Two key risk genes for neurodegenerative disorders, *APOE* for Alzheimer's disease and *SNCA* for Parkinson's disease, exhibit strongly negative MMCs, with higher expression levels in association cortex relative to sensory cortex (*APOE*: MMC $= -0.64$, $P < 10^{-15}$; *SNCA*: MMC $= -0.80$, $P < 10^{-42}$). **a,** *APOE* is a leading risk gene for Alzheimer's disease. The $\varepsilon 4$ allele of *APOE* is the largest genetic risk factor for late-onset Alzheimer's disease. **b,** *SNCA* (*PARK1*/*PARK4*) is a key risk gene for Parkinson's disease. Duplication of *SNCA* is risk factor for familial Parkinson's disease with dominant inheritance. *SNCA* codes for the alpha-synuclein protein which is the primary component of Lewy bodies, which are a biomarker of Parkinson's disease.